BRAIN
ORIGINAL ARTICLE

Tumour necrosis factor blockade after asphyxia in foetal sheep ameliorates cystic white matter injury

Christopher A. Lear,† Benjamin A. Lear,† Joanne O. Davidson, Jialin Sae-Jiw, Johanna M. Lloyd, Simerdeep K. Dhillon, Alistair J. Gunn and Laura Bennet

†These authors contributed equally to this work.

Cystic white matter injury is highly associated with severe neurodevelopmental disability and cerebral palsy in preterm infants, yet its pathogenesis remains poorly understood and there is no established treatment. In the present study, we tested the hypothesis that slowly evolving cystic white matter injury after hypoxia-ischaemia is mediated by programmed necrosis initiated by tumour necrosis factor. Tumour necrosis factor blockade was begun 3 days after hypoxia-ischaemia to target the tertiary phase of injury, when most secondary cell death is thought to be complete.

Chronically instrumented preterm foetal sheep (0.7 gestation) received 25 min of hypoxia-ischaemia induced by complete umbilical cord occlusion or sham-umbilical cord occlusion (controls, $n = 10$), followed by intracerebroventricular infusion of the soluble TNF inhibitor, Etanercept, at 3, 8 and 13 days after umbilical cord occlusion ($n = 9$) or vehicle ($n = 9$). Foetal brains were processed for histology at 21 days after umbilical cord occlusion.

Umbilical cord occlusion with vehicle was associated with a spectrum of macroscopic white matter degeneration, including white matter atrophy, ventriculomegaly and overt temporal lobe cystic white matter injury. Oligodendrocyte maturational arrest and impaired labelling of myelin proteins, characteristic of diffuse white matter injury, was observed in the parietal lobe and surrounding the cystic lesions in the temporal lobe. Etanercept markedly attenuated cystic white matter injury on the side of the intracerebroventricular infusion, with partial contralateral protection. Further, Etanercept improved oligodendrocyte maturation and labelling of myelin proteins in the temporal and parietal lobes.

The present study shows that cystic white matter injury reflects late-onset tertiary cell death mediated by delayed neuroinflammation through the tumour necrosis factor pathway. Delayed tumour necrosis factor blockade markedly attenuated cystic white matter injury and restored oligodendrocyte maturation and deficits in myelin protein expression. These data suggest that delayed tumour necrosis factor blockade may represent a viable therapeutic strategy to reduce the risk of cystic and diffuse white matter injury and potentially cerebral palsy after preterm birth, with a surprisingly wide therapeutic window.

The Fetal Physiology and Neuroscience Group, Department of Physiology, The University of Auckland, Auckland, New Zealand

Correspondence to: Laura Bennet
Private Bag 92019, Auckland 1142, New Zealand
E-mail: l.bennet@auckland.ac.nz

Keywords: hypoxia-ischaemia; periventricular leukomalacia; preterm; Etanercept; white matter injury

Received April 03, 2022. Revised July 20, 2022. Accepted August 23, 2022. Advance access publication September 10, 2022

Introduction

Preterm birth is associated with high rates of neurodevelopmental disability and is implicated in over a third of all cases of cerebral palsy.[1] Although the incidence of severe cystic white matter injury (WMI) also known as cystic periventricular leukomalacia is gradually falling,[2] it remains strongly associated with severe disabilities such as cerebral palsy.[3–7] Although preterm brain injury is multifactorial, hypoxia-ischaemia (HI) before or during birth including events such as placental abruption, placenta previa and cord prolapse or in association with placental insufficiency remains associated with neurodevelopmental disability.[8–10] The risk of HI increases with decreasing gestational age. For example, in a study of 8334 live singleton preterm births, the rate of hypoxic-ischaemic encephalopathy increased from 30.8 per 1000 births at 28–36 weeks gestation to 119.9 at <28 weeks.[10]

We have recently shown that severe HI at preterm equivalent gestation in foetal sheep leads to a slowly evolving pattern of cystic WMI, such that WMI was initially characterized by diffuse disruption of myelin and selective oligodendrocyte death at 3–7 days after HI, followed by development of severe, cystic WMI mainly in the temporal lobe by 14–21 days after HI.[11] Diffuse (non-cystic) WMI was seen in the periphery of the area of severe WMI in the temporal lobe and in the parietal lobe,[11] and characterized by astrogliosis, maturational arrest of oligodendrocytes and impaired myelin protein labelling, similar to previous studies.[9,12,13]

The strikingly slow evolution of cystic WMI in the foetal sheep in our previous study mirrors the appearance of cystic WMI on ultrasonography in human preterm neonates.[7,14] These data suggest that substantial white matter cell death can occur in the 'tertiary' phase of injury, from about 72 h after HI onwards.[15] In neonatal rodents there is evidence that programmed necrosis is initiated by membrane-bound death receptor activation by the tumour necrosis factor (TNF) family of cytokines,[16] and can evolve over weeks after HI.[17] Consistent with these data, in the preterm foetal sheep no apoptotic cell death or caspase-3 expression was seen before emergence of cystic WMI, and cystic injury was preceded by exuberant local microgliosis.[11]

We therefore tested the hypothesis that delayed TNF blockade within the tertiary phase of injury after HI would prevent tertiary white matter cell death, and thereby reduce the severity of cystic WMI and promote oligodendrocyte maturation and recovery of myelin protein labelling. Severe HI was induced via umbilical cord occlusion (UCO) in preterm foetal sheep at 0.7 of gestation. Foetal sheep were allowed to recover for 21 days after UCO. In sheep, this period broadly spans equivalent human brain maturation from 30 weeks of gestation to full-term.[18,19] The highly specific soluble TNF inhibitor, Etanercept, was administered by intracerebroventricular infusion centrally at 3, 8 and 13 days after UCO. Etanercept is a genetically engineered fusion protein of the extracellular portion of TNF receptor 2 linked to the Fc portion of IgG1.[20] Etanercept binds TNF preventing it from interacting with cell surface TNF receptors and thereby renders it biologically inactive.[20] It is a large (150 kDa) fusion protein[20] that is unlikely to cross the blood–brain barrier.[21]

Materials and methods

Ethical approval

All procedures were approved by the Animal Ethics Committee of the University of Auckland, and carried out in accordance with the New Zealand Animal Welfare Act 1999 and the University of Auckland's Code of Ethical Conduct for the use of animals for teaching and research, approved by the Ministry of Primary Industries, Government of New Zealand. This paper is compliant with the ARRIVE guidelines for reported animal research.[22]

Surgical procedures

In total, 28 Romney/Suffolk foetal sheep were surgically instrumented at 98–100 days of gestation (term is 147 days) as previously described.[23] Ewes were given long-acting oxytetracycline (20 mg/kg, Phoenix Pharm Distributors) intramuscularly 30 min before surgery for antibiotic prophylaxis. Anaesthesia was induced by intravenous injection of propofol (5 mg/kg, AstraZeneca) and general anaesthesia was maintained using 2–3% isoflurane in oxygen. The depth of anaesthesia, maternal heart rate and respiration were constantly monitored by trained anaesthetic staff. Ewes received a constant infusion of isotonic saline (~250 ml/h) to maintain fluid balance.

A midline abdominal incision was made to expose the uterus, and the foetus was partially exteriorized for instrumentation. Polyvinyl catheters (SteriHealth) were placed in the left saphenous artery to measure arterial blood pressure and the right brachial artery for pre-ductal blood sampling. An additional catheter was placed into the amniotic sac for measurement of pressure within the amniotic space. Two electrodes (AS633–5SSF, Cooner Wire) were placed subcutaneously over the right shoulder and at the level of the left fifth intercostal space to measure the foetal ECG. An intracerebroventricular catheter was placed into the right lateral ventricle (6 mm anterior and 4 mm lateral to bregma). Finally, an inflatable silicone occluder was placed around the umbilical cord to facilitate UCOs (OC18HD, In Vivo Metric).

Gentamicin was administered into the amniotic sac (80 mg, Pfizer) before the uterus was closed. The maternal midline skin incision was infiltrated with a local analgesic, 10 ml of 0.5% bupivacaine plus adrenaline (AstraZeneca) to provide long-acting analgesia. All foetal leads were exteriorized through the maternal flank, and a maternal long saphenous vein was catheterized for postoperative care and euthanasia.

Postoperative care

Following surgery, ewes were housed together in separate metabolic cages with *ad libitum* access to food and water. Rooms were temperature and humidity controlled (16 ± 1°C, humidity 50 ± 10%) with a 12-h light/dark cycle (light 0600 to 1800). Ewes were given daily intravenous antibiotics (600 mg benzylpenicillin sodium, Novartis, and 80 mg gentamicin) for 4 days after surgery. Foetal catheters were maintained patent with continuous infusion of heparinized saline (20 U/ml at 0.2 ml/h).

Data acquisition and recordings

Foetal mean arterial pressure and ECG were recorded continuously from 24 h before UCO.[24] All signals were processed and initially digitized at a sampling rate of 4096 Hz before being decimated to lower sampling rates and stored using customized LabVIEW-based data acquisition software (National Instruments). Foetal arterial blood pressure was recorded using Novatrans III Gold, MX860 pressure transducers (Medex) and corrected for maternal position by subtraction of amniotic fluid pressure. The pressure signals were amplified 500×, low-pass filtered with a fifth-order Butterworth filter set at 20 Hz and saved at 64 Hz. The raw ECG signal was analogue filtered with a first-order high-pass filter set at

1 Hz and an eighth-order low-pass Bessel filter set at 100 Hz and saved at 1024 Hz.

Experimental protocol

Experiments began between 0900 and 0930, 4–6 days after surgery when foetuses were at 104–105 days of gestation. Foetuses were randomly assigned to receive UCO plus delayed artificial cerebrospinal fluid (UCO-vehicle, $n = 9$), UCO plus delayed Etanercept treatment (UCO-Etanercept, $n = 9$) or sham-UCO plus delayed artificial cerebrospinal fluid (control, $n = 10$). HI was induced by complete UCO for 25 min and UCO was ended early if mean arterial pressure fell below 8 mmHg or asystole developed.[25] Control foetuses received no occlusion. Etanercept was administered via intracerebroventricular infusion at 72, 192 and 312 h (3, 8 and 13 days) after the end of UCO. Etanercept (1.0 mg) was dissolved in 0.5 ml of sterile artificial cerebrospinal fluid and infused over a period of 4 h (125 µl/h). Both control and UCO-vehicle groups received the same volume of artificial CSF. The start of Etanercept infusions was designed to correspond with the estimated beginning of the tertiary phase of injury from 72 h onwards.[15] The spacing between the infusions was chosen to broadly reflect the systemic half-life of Etanercept of 4–5 days.[20,26] The dose of Etanercept was extrapolated and adjusted for relative body and brain size from studies in humans and rats.[27,28]

Ewes and foetuses were killed 21 days after UCO by an overdose of sodium pentobarbitone given intravenously to the ewe (9 g Pentobarb 300, Provet New Zealand). This method is consistent with the Animal Welfare Act of New Zealand.

Arterial blood samples

Foetal arterial blood samples (0.3 ml) were taken before the start of the experiment, at 5 and 17 min during UCO, and at 2, 4 and 6 h after occlusion, then daily thereafter between 0830 and 0930. Blood samples were analysed for pH and blood gases (ABL 800, Radiometer) and glucose and lactate levels (YSI model 2300). Selected time points from 1 to 21 days after UCO are presented for brevity.

Histological preparation

At post-mortem, foetal brains were perfusion fixed *in situ* with 10% phosphate-buffered formalin and remained in formalin for 1 week before being processed and paraffin embedded. 10-µm thick coronal sections were cut using a rotary microtome (RM2235, Leica Microsystems). Sections were taken 17 mm anterior to stereotaxic zero to examine the white matter of the parietal and temporal lobes.[29] Slides were dewaxed in xylene and rehydrated in decreasing concentrations of ethanol and subsequently washed in 0.1 mol/l phosphate-buffered saline. To examine macroscopic structural integrity two sections per animal were stained with both thionine (Scharlau) and acid fuchsin (Sigma-Aldrich) before being dehydrated in increasing concentrations of alcohol followed by xylene and mounted with coverslips.

Additional sections (two sections per animal per antibody) were labelled for immunohistochemistry. Following dewaxing and rehydration as before, antigen retrieval was performed in citrate buffer with the 2100 Antigen Retriever (Aptum Biologics). Endogenous peroxidase was quenched by incubation in 1% H_2O_2 in methanol or in phosphate-buffered saline for Olig-2. Blocking was performed for 1 h at room temperature in 3% normal goat serum. Sections were labelled with monoclonal primary antibodies at 1:200 concentration: rabbit anti-oligodendrocyte transcription factor 2 (Olig-2, Merck-Millipore), mouse anti-adenomatous polyposis coli clone CC1 (CC1, Merk-Millipore), mouse anti-2′,3′-cyclic-nucleotide 3′-phosphodiesterase (CNPase, Merck-Millipore), rabbit anti-myelin basic protein (MBP, Merck-Millipore), goat anti-ionized calcium-binding adapter molecule 1 (Iba-1, Abcam) and rabbit anti-glial fibrillary acidic protein (GFAP, Abcam) overnight at 4°C. Sections were incubated for 3 h with the species appropriate biotin-conjugated monoclonal secondary antibody (Vector Laboratories) at 1:200 dilution in 3% normal goat serum. Slides were incubated in ExtrAvidin (Sigma-Aldrich) at a dilution of 1:200 in normal goat serum for 2 h and then reacted with diaminobenzidine tetrachloride (Sigma-Aldrich). The reaction was halted by immersion in phosphate-buffered saline. Slides were dehydrated in increasing concentrations of alcohol followed by xylene and mounted with coverslips.

White matter and cystic lesion area analysis

Macroscopic examination of the structural integrity of the white matter of the parietal and temporal lobes was performed on sections stained with acid fuchsin/thionine by a blinded assessor. Blinding across the study was achieved by independent coding of slides and data files. Macroscopic examination was performed on whole section images taken on a Zeiss Axio Imager Z2 microscope with automated motorized stage (Carl Zeiss AG). Serial images were collected at ×2.5 magnification and collated using VSlide stitching software (MetaSystems, Altlussheim, Germany). Total white matter and ventricle area was measured using ImageJ software (National Institutes of Health, Bethesda, MD, USA). The total white matter area was measured across all continuous white matter structures of the parietal and temporal lobes of both hemispheres, including the intragyral and periventricular regions and the corpus callosum. Macroscopic cystic white matter lesions were identified in the UCO groups, most commonly in the temporal lobe, as previously described.[11] The area of each identified lesion was measured, and the area was subtracted from the total white matter area to give a final intact white matter area. For the purpose of this analysis, cystic tissue was defined as macroscopically evident irregular architecture or macroscopic cellular loss.[30,31]

Temporal and parietal lobe microscopy

Images of Olig2, CC1, CNPase, MBP, Iba-1 and GFAP labelled tissue were taken from two regions in the temporal lobe and three regions in the parietal lobe at ×20 magnification by a blinded assessor on an Eclipse 80i microscope (Nikon Corporation). These five regions were imaged on both left and right cerebral hemispheres. The locations from which images were taken are shown in Fig. 1. In the temporal lobe, the first image (temporal white matter 1, TWM1) was taken from the centre of the temporal lobe white matter. This represents the region with the most severe injury at 21 days after UCO, including the appearance of cystic white matter lesions.[11] The second image (TWM2) was taken from the superomedial white matter of the temporal lobe, which represents a less severely injured region.[11] The temporal lobe cystic white matter lesions were surrounded by a border of Iba-1-positive and GFAP-positive cells, TWM2 was positioned outside of this border to ensure that it was in a less severely injured region and did not include the dense cellular border. Images from representative regions were taken in animals that had no identifiable cystic lesions, including all control animals. In the parietal lobe, images were taken from the first and second intragyral white matter (IGWM1, IGWM2) and the periventricular white matter regions (PVWM) as shown in Fig. 1.

All analyses were performed by a blinded assessor. Cell counts for total oligodendrocytes (Olig2-positve cells), mature oligodendrocytes (CC1-positive cells), microglia (Iba-1 positive cells) and astrocytes (GFAP-positive cells) were performed by manual counts using ImageJ (National Institutes of Health). Two sections per animal per antibody were included. Images from both left and right hemispheres were counted and averaged. Microglia showing either an amoeboid or ramified morphology were included. For qualitative purposes, amoeboid microglia were considered to have a spherical cell body, intense or more condensed labelling and displaying one or zero visible processes. Ramified microglia were considered to have elongated cell bodies, less intense labelling and displaying multiple processes. The area fractions of MBP-positive and CNPase-positive labelling were quantified using ImageJ (National Institutes of Health).

Statistical analysis

Statistical analysis was performed using SPSS v.28 (SPSS, Chicago, IL, USA). Histological outcomes in the parietal lobe regions (IGWM1, IGWM2 and PVWM) were assessed using two-way ANOVA with group as the independent factor and area treated as repeated measures. The temporal lobe regions were assessed separately using one-way ANOVA with group as the independent factor. Analysis of post-mortem and biochemistry data were assessed by one-way ANOVA with group as the independent factor. If a significant group effect was found in these analyses, the Fisher's protected least significant difference *post hoc* test was performed in addition. Statistical significance was accepted when $P < 0.05$. Data are mean ± SEM.

Data availability

The data that support the findings of this study are available from the corresponding author on reasonable request.

Results

Baseline and umbilical cord occlusion

All foetuses across all groups had normal physiological and arterial blood gas parameters by our laboratory standards before the start of experiments. There were no significant differences in any physiological parameters between the groups before experiments. UCO was associated with sustained bradycardia, with progressive, severe arterial hypotension, hypoxemia, hypoglycaemia and respiratory and metabolic acidosis (Table 1). There were no differences in the duration of occlusions or the severity of hypotension at the end of occlusion between the UCO-vehicle (24:53 min ± 4 s, 12.1 ± 0.9 mmHg) and UCO-Etanercept groups (24:33 min ± 18 s, 11.3 ± 0.8 mmHg). There was also no difference in the severity of hypotension when assessed as either the area of arterial pressure under 20 mmHg ($P = 0.484$) or the time spent below 20 mmHg ($P = 0.110$) between groups (data not shown). Foetal heart rate and mean arterial pressure recovered rapidly after the end of occlusion. Foetal demographics and post-mortem data are presented in Table 2.

TNF blockade-reduced temporal lobe cystic WMI

A spectrum of macroscopic WMI was observed in both UCO groups as detailed in Table 3. In the UCO-vehicle group, 4/9 foetuses developed marked white matter atrophy and ventriculomegaly. Cystic white matter lesions were observed in an overlapping group of 5/9 foetuses. The temporal lobe white matter was the most frequently affected region, including two foetuses that showed near complete destruction of all white matter in the temporal lobe (Fig. 1 and Table 3). When cystic lesions were observed, they were associated with a marked reduction in all cellular elements within the core of the lesions, including a loss of total (Olig2-positive) and mature (CC1-positive) oligodendrocytes, complete loss of or highly fragmented MBP-positive and CNPase-positive myelin protein labelling. These areas were sparsely populated with intensely labelled Iba-1-positive amoeboid microglia, with a dense border of Iba-1-positive microglia and GFAP-positive astrocytes surrounding the lesions.

A similar spectrum of macroscopic injury was observed in the UCO-Etanercept group, but with reduced severity (Fig. 1 and Table 3). While temporal lobe cystic lesions were predominantly observed bilaterally in the UCO-vehicle group, no cystic lesions were seen in the UCO-Etanercept group in the temporal lobes ipsilateral to the intracerebroventricular infusion. Strikingly, the unilateral lesions in the UCO-Etanercept group were always observed contralateral to the hemisphere that received the Etanercept infusion. Fewer foetuses (two versus four foetuses) in the UCO-Etanercept developed a pattern of white matter atrophy and ventriculomegaly, representing the most severe pattern of injury.[11,15] Those that did develop this pattern showed markedly less loss of intact white matter area, albeit with a modest increase in the area of cystic lesions compared with the UCO-vehicle group (Table 3).

Intact white matter area was reduced in the UCO-vehicle group compared with controls ($P = 0.007$), with a corresponding increase in lateral ventricle area in both the UCO-vehicle ($P = 0.005$) and the UCO-Etanercept groups ($P = 0.002$) compared with controls (Table 2). Intact white matter area in the UCO-Etanercept group was intermediate between controls and the UCO-vehicle group ($P = 0.209$ and $P = 0.120$, respectively; Table 2). No relationship was found between the severity of hypotension during UCO and the intact white matter area in the UCO-vehicle and UCO-Etanercept groups when assessed as either the area of arterial pressure under 20 mmHg ($P = 0.300$, $R^2 = 0.067$, $n = 18$; Fig. 1) or the time spent below 20 mmHg ($P = 0.141$, $R^2 = 0.130$, $n = 18$, data not shown).

We further assessed the severity of immunohistological injury in the centre of the temporal lobe (TWM1 region), as this region showed the most severe injury, including most cystic lesions (Figs 2 and 3). A significant effect of group was observed for Olig2 ($P = 0.021$), CC1 ($P = 0.003$), MBP ($P = 0.000$) and CNPase ($P = 0.000$) outcomes in the TWM1 region but not for Iba-1 ($P = 0.796$) or GFAP ($P = 0.052$). Further testing revealed that the UCO-vehicle group showed a reduction in the numbers of total (Olig2-positive, $P = 0.031$), and mature oligodendrocytes (CC1-positive, $P = 0.001$) and a reduction in the area fraction of MBP-positive ($P = 0.000$) and CNPase-positive myelin protein labelling ($P = 0.000$) compared with controls. TNF blockade in the UCO-Etanercept group restored the numbers of total oligodendrocytes to control levels (Olig2-positive, $P = 0.533$ versus control, $P = 0.009$ versus UCO-vehicle) and partially restored the area fraction of MBP-positive labelling in the TWM1 region, leading to a higher area fraction compared with the UCO-vehicle group ($P = 0.006$) but a lower area fraction compared with controls ($P = 0.035$). TNF blockade did not alter the loss of mature oligodendrocytes (CC1-positive, $P = 0.018$ versus controls, $P = 0.209$ versus UCO-vehicle), nor the reduction in the area fraction of CNPase-positive labelling in the TWM1 region ($P = 0.000$ versus controls, $P = 0.318$ versus UCO-vehicle).

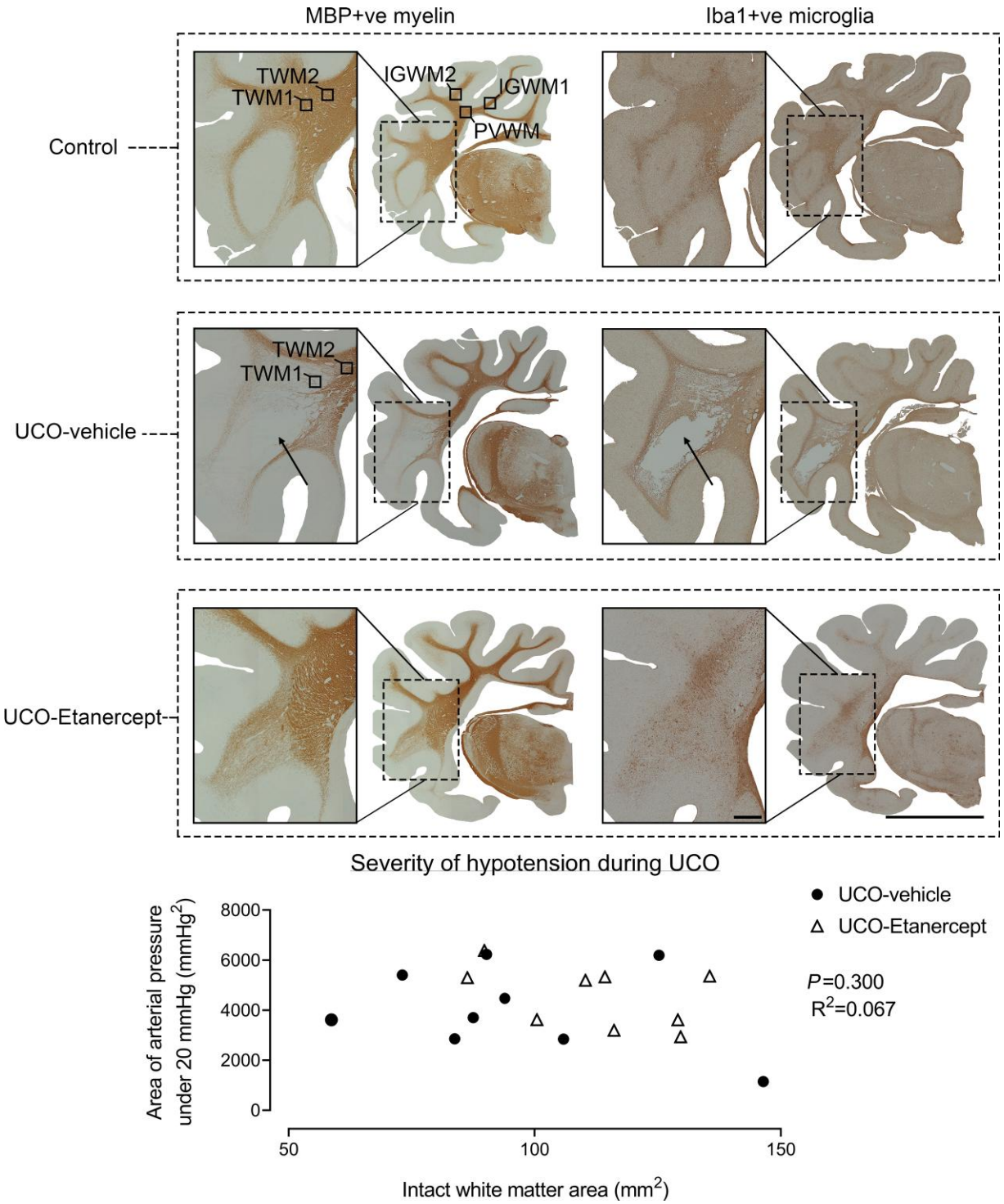

Figure 1 Macroscopic WMI. Examples of coronal sections of the right hemisphere and enlargement of the temporal lobe after 21 days recovery from UCO labelled for MBP-positive myelin proteins (*left column*) and Iba-1-positive microglia (*right column*). Note the cystic white matter lesions observed in the temporal lobe in the UCO-vehicle group (arrows), and absence of cystic lesions in the control and UCO-Etanercept groups. Images were taken at ×2.5 magnification. The *top left* coronal section shows the five white matter regions assessed for microscopic analysis. Scale bar = 10 mm for the right hemisphere and 1 mm for enlarged sections. *Bottom* graph shows that no relationship was found between the severity of hypotension during UCO (assessed as the area of arterial pressure under 20 mmHg) and the intact white matter area.

Due to the unilateral distribution of cystic WMI in the UCO-Etanercept group, we performed targeted exploratory analysis on the numbers of total oligodendrocytes (Olig2-positive) in the centre of the temporal lobe (TWM1) in which the two hemispheres were included as a repeated measure for ANOVA analysis (data not shown). A significant interaction between group and hemisphere in the numbers of total oligodendrocytes was observed in the TWM1 region ($P = 0.004$). In the UCO-Etanercept group, further paired

Table 1 Foetal pH, blood gases and metabolites

	Group	Baseline	UCO (5 min)	UCO (17 min)	+2 h	+4 h	+6 h	+1 day	+3 days	+7 days	+14 days	+21 days
pH	Control	7.36 ± 0.01	7.36 ± 0.01	7.36 ± 0.01	7.36 ± 0.01	7.35 ± 0.01	7.35 ± 0.01	7.35 ± 0.01	7.34 ± 0.01	7.35 ± 0.01	7.34 ± 0.01	7.33 ± 0.01
	UCO-vehicle	7.35 ± 0.01	7.03 ± 0.01*	6.84 ± 0.01*	7.29 ± 0.02*	7.38 ± 0.01	7.40 ± 0.01*	7.36 ± 0.01	7.36 ± 0.01	7.36 ± 0.01	7.35 ± 0.01	7.36 ± 0.01
	UCO-Etanercept	7.36 ± 0.01	7.05 ± 0.01*	6.85 ± 0.01*	7.32 ± 0.01*	7.38 ± 0.01	7.39 ± 0.01*	7.37 ± 0.01	7.36 ± 0.00	7.37 ± 0.01	7.35 ± 0.01	7.35 ± 0.01
p_aCO_2 (mmHg)	Control	48.5 ± 0.7	47.1 ± 0.8	46.6 ± 0.8	47.3 ± 0.9	46.1 ± 1.1	46.7 ± 0.9	47.1 ± 0.7	48.4 ± 0.8	49.1 ± 0.8	48.6 ± 1.0	49.4 ± 1.2
	UCO-vehicle	50.7 ± 1.4	99.7 ± 2.6*	136.4 ± 6.0*	47.8 ± 0.8	47.7 ± 1.1	48.5 ± 0.7	46.3 ± 1.4	46.8 ± 1.5	49.2 ± 1.8	50.7 ± 1.4	48.6 ± 1.1
	UCO-Etanercept	52.7 ± 1.3	94.7 ± 3.4*	131.4 ± 2.2*	50.6 ± 0.8*	48.6 ± 0.7*	50.6 ± 1.2	49.0 ± 1.2	50.7 ± 0.5	50.5 ± 1.4	51.0 ± 1.1	51.8 ± 1.4
p_aO_2 (mmHg)	Control	25.6 ± 0.6	24.6 ± 0.7	24.3 ± 0.6	25.5 ± 0.7	24.9 ± 0.5	25.7 ± 0.7	26.2 ± 0.8	27.0 ± 0.7	25.3 ± 1.1	26.0 ± 1.4	22.6 ± 1.3
	UCO-vehicle	24.7 ± 0.8	6.6 ± 0.4*	9.5 ± 1.2*	27.2 ± 1.2	23.5 ± 1.0	25.4 ± 1.0	29.1 ± 1.0*	31.1 ± 1.2*	29.4 ± 1.5*	28.4 ± 1.2	26.5 ± 1.8*
	UCO-Etanercept	25.8 ± 1.1	8.3 ± 0.7*	13.1 ± 1.4*	27.8 ± 1.4*	26.1 ± 0.9	27.9 ± 1.1	30.2 ± 0.6*	30.0 ± 0.6*	29.0 ± 1.1*	28.8 ± 1.3	26.5 ± 1.2*
Hct (%)	Control	27.2 ± 0.7	26.2 ± 0.8	26.1 ± 0.9	26.7 ± 0.7	28.2 ± 0.2	25.9 ± 0.9	26.9 ± 0.8	29.4 ± 1.4	31.6 ± 1.8	31.3 ± 1.3	31.4 ± 0.8
	UCO-vehicle	26.2 ± 0.7	27.8 ± 1.1	28.2 ± 0.8	28.1 ± 0.7	27.4 ± 0.5	27.7 ± 0.8	29.0 ± 0.5	30.2 ± 2.2	33.6 ± 3.7	35.2 ± 4.4	30.2 ± 0.3
	UCO-Etanercept	26.5 ± 1.3	27.6 ± 1.0	26.6 ± 1.4	28.7 ± 1.4	27.5 ± 1.3	27.5 ± 1.3	28.0 ± 1.6	26.3 ± 1.4	27.3 ± 1.6	27.7 ± 1.8	28.9 ± 2.0
O_2ct (mmol/l)	Control	3.7 ± 0.1	3.4 ± 0.1	3.3 ± 0.2	3.6 ± 0.1	3.2 ± 0.1	3.4 ± 0.2	3.7 ± 0.2	3.9 ± 0.1	3.9 ± 0.2	3.9 ± 0.2	3.3 ± 0.3
	UCO-vehicle	3.6 ± 0.1	0.4 ± 0.1*	0.5 ± 0.1*	4.3 ± 0.3*	3.6 ± 0.2 *	2.7 ± 0.8*	4.5 ± 0.1*	4.6 ± 0.2	4.6 ± 0.2	4.5 ± 0.2	4.2 ± 0.2
	UCO-Etanercept	3.5 ± 0.2	0.4 ± 0.0*	0.5 ± 0.1*	4.1 ± 0.3	3.8 ± 0.2*	4.0 ± 0.2	4.3 ± 0.2	4.4 ± 0.2	4.2 ± 0.3	4.1 ± 0.3	4.0 ± 0.4
Lactate (mmol/l)	Control	0.9 ± 0.1	0.9 ± 0.03	0.9 ± 0.1	0.9 ± 0.0	0.9 ± 0.0	1.0 ± 0.0	0.9 ± 0.1	0.8 ± 0.04	0.9 ± 0.0	0.8 ± 0.0	1.1 ± 0.1
	UCO-vehicle	0.8 ± 0.1	3.9 ± 0.2*	6.2 ± 0.3*	4.8 ± 0.7*	3.0 ± 0.5*	2.1 ± 0.2*	1.5 ± 0.2*	0.9 ± 0.1	0.7 ± 0.0	0.8 ± 0.0	0.8 ± 0.0
	UCO-Etanercept	0.8 ± 0.1	3.7 ± 0.2*	5.8 ± 0.7*	4.4 ± 0.5*	2.4 ± 0.5*	2.4 ± 0.5*	1.0 ± 0.1	0.9 ± 0.1	0.8 ± 0.1	0.9 ± 0.1	0.9 ± 0.1
Glucose (mmol/l)	Control	1.1 ± 0.1	1.0 ± 0.0	1.0 ± 0.1	1.2 ± 0.1	1.1 ± 0.1	1.2 ± 0.1	1.1 ± 0.1	1.0 ± 0.1	1.0 ± 0.1	0.8 ± 0.1	0.8 ± 0.1
	UCO-vehicle	1.0 ± 0.1	0.4 ± 0.1*	0.6 ± 0.1*	1.3 ± 0.1	1.3 ± 0.1	1.4 ± 0.1	1.4 ± 0.1	1.1 ± 0.1	0.9 ± 0.1	0.9 ± 0.1	0.9 ± 0.0
	UCO-Etanercept	1.0 ± 0.1	0.4 ± 0.1*	0.6 ± 0.1*	1.4 ± 0.1*	1.3 ± 0.1	1.5 ± 0.1	1.2 ± 0.1	1.3 ± 0.1	1.1 ± 0.1	1.1 ± 0.1	1.0 ± 0.1

Hct, haematocrit; O_2ct, arterial oxygen content; p_aCO_2, arterial partial pressure of carbon dioxide; p_aO_2, arterial partial pressure of oxygen. Data are mean ± SEM.
*$P < 0.05$ versus control.

Table 2 Area measurements, foetal demographics and post-mortem weights

Group	Intact white matter area (mm^2)	Lateral ventricle area (mm^2)	Brain (g)	Sex (F/M)	Body weight (g)	Heart (g)	Lungs (g)	Liver (g)	Kidneys (g)	Spleen (g)
Control	125.3 ± 6.3	46.4 ± 3.1	39.5 ± 0.9	4/6	3224.2 ± 204.3	22.3 ± 0.8	88.9 ± 6.4	112.8 ± 10.4	12.4 ± 0.7	7.8 ± 0.9
UCO-vehicle	96.1 ± 8.9*	69.4 ± 6.2*	32.5 ± 1.7*	6/3	3182.2 ± 157.4	20.8 ± 0.4	44.3 ± 5.6*	89.9 ± 6.8	11.3 ± 0.8	6.1 ± 0.5
UCO-Etanercept	114.7 ± 5.5	71.6 ± 6.5*	35.5 ± 1.4*	8/1	3286.3 ± 195.8	22.9 ± 1.1	50.3 ± 6.9*	122.9 ± 13.6	11.5 ± 0.9	6.8 ± 0.6

Data are mean ± SEM. F = female; M = male.
*$P < 0.05$ versus control.

t-tests showed a higher number of total oligodendrocytes (Olig2-positive) in the TWM1 region ipsilateral to the intracerebroventricular catheter than that on the contralateral side ($P = 0.003$). No difference between ipsilateral and contralateral TWM1 regions were observed in the UCO-vehicle ($P = 0.541$) or control groups ($P = 0.707$).

TNF blockade-reduced temporal lobe diffuse white matter injury

In the superomedial aspect of the temporal lobe white matter (TWM2 region, positioned at the periphery of the most common site of cystic WMI), we observed moderately severe diffuse WMI (Figs 2 and 3). A significant effect of group was observed for Olig2 ($P = 0.000$), CC1 ($P = 0.002$), MBP ($P = 0.000$), CNPase ($P = 0.000$), Iba-1 ($P = 0.001$) and GFAP ($P = 0.019$) outcomes in the TWM2 region. Further testing revealed that the UCO-vehicle group showed a reduction in the numbers of mature oligodendrocytes (CC1-positive, $P = 0.001$), the area fraction of MBP-positive ($P = 0.000$) and CNPase-positive myelin protein labelling ($P = 0.000$), and increased numbers of microglia (Iba-1-positive, $P = 0.036$) and astrocytes (GFAP-positive, $P = 0.045$) in the TWM2 region compared with controls. Numbers of total oligodendrocytes were not different between the UCO-vehicle and control groups (Olig2-positive, $P = 0.164$). TNF blockade in the UCO-Etanercept group restored numbers of mature oligodendrocytes (CC1-positive, $P = 0.876$ versus control, $P = 0.002$ versus UCO-vehicle), the area fraction of MBP-positive labelling ($P = 0.566$ versus control, $P = 0.000$ versus UCO-vehicle) and numbers of astrocytes (GFAP-positive, $P = 0.328$ versus control, $P = 0.006$ versus UCO-vehicle) back to control levels in the TWM2 region. TNF blockade was associated with increased total numbers of oligodendrocytes (Olig2-positive) compared with both UCO-vehicle ($P = 0.000$) and control groups ($P = 0.000$), and a marked reduction in numbers of microglia (Iba-1-positive) compared with both the UCO-vehicle group ($P = 0.000$) and controls ($P = 0.027$). TNF blockade did not improve the area fraction of CNPase-positive labelling in the TWM2 region ($P = 0.000$ versus control, $P = 0.573$ versus UCO-vehicle).

Morphologically, UCO was associated with impaired labelling of MBP-positive and CNPase-positive myelin proteins in the temporal lobe white matter. Myelin protein fibres appeared shorter, more fragmented and overall more sparsely labelled compared with controls (Figs 1 and 2). This was most severe in the centre of the temporal lobe (including the TWM1 region) but still observed in the periphery of the temporal lobe (including the TWM2 region). High-magnification (×40) images of MBP-positive and CNPase-positive myelin protein labelling in the TWM2 region are shown in Supplementary Fig. 1. Consistent with the quantitative area fraction findings, both MBP-positive and CNPase-positive labelling in the UCO-Etanercept group showed less marked morphological disruption compared with the UCO-vehicle group (Figs 1 and 2). In the UCO-vehicle group, a high proportion of microglia showed an amoeboid morphology, while those in the control and UCO-Etanercept group showed a higher proportion of ramified morphologies in the TWM2 regions (Fig. 3).

TNF blockade mitigated parietal lobe white matter injury

The three parietal lobe white matter regions (IGWM1/2 and PVWM) showed milder diffuse WMI after UCO in contrast with the severe injury observed in the temporal lobe (Figs 4 and 5). A significant effect of group across the three regions (two-way ANOVA) was observed for CC1 ($P = 0.018$), CNPase ($P = 0.02$), Iba-1 ($P = 0.018$) and GFAP ($P = 0.024$) outcomes, but not for Olig2 ($P = 0.968$) or MBP ($P = 0.802$). Further testing revealed that the UCO-vehicle group showed a reduction in the numbers of mature oligodendrocytes (CC1-positive, $P = 0.02$) and the area fraction of CNPase-positive myelin protein labelling ($P = 0.006$) and increased numbers of microglia (Iba-1-positive, $P = 0.02$) in the IGWM1/2 and PVWM regions compared with controls. TNF blockade in the UCO-Etanercept group restored the numbers of mature oligodendrocytes (CC1-positive, $P = 0.785$ versus control, $P = 0.01$ versus UCO-vehicle) and the numbers of microglia (Iba-1-positive, $P = 0.635$ versus control, $P = 0.008$ versus UCO-vehicle) back to control levels. TNF blockade additionally reduced the numbers of astrocytes (GFAP-positive) compared with the UCO-vehicle group ($P = 0.008$) but not compared with controls ($P = 0.069$). The area fraction of CNPase-positive myelin protein labelling in the UCO-Etanercept group was not significantly different from either the control ($P = 0.129$) or UCO-vehicle groups in the parietal lobe regions ($P = 0.169$).

Morphologically, both MBP-positive and CNPase-positive myelin protein labelling across the parietal lobe in the UCO-vehicle and UCO-Etanercept group appeared intact and similar in appearance to that in the control group (Fig. 4). High-magnification (×40) images of MBP-positive and CNPase-positive myelin protein labelling in the IGWM2 region are shown in Supplementary Fig. 1. The morphology of Iba-1 positive microglia within the three parietal lobe regions was similar across all groups, predominantly showing ramified morphology (Fig. 5). Likewise, GFAP-positive astrocytes appeared morphologically similar across all groups within the three parietal lobe regions (Fig. 5).

Discussion

The present study demonstrates for the first time that delayed TNF blockade with the large fusion protein, Etanercept, can attenuate macroscopic and cystic WMI and improve oligodendrocyte maturation after HI in preterm foetal sheep. This finding strongly supports the hypothesis that inflammatory events in the tertiary

Table 3 Macroscopic patterns of WMI

Number with pattern	Additional features	Intact white matter area (mm^2)	Ventricle area (mm^2)	Cystic lesion area (mm^2)
Control outcomes				
Control 10 foetuses	-	125.3 ± 6.3	46.4 ± 3.1	-
White matter atrophy and ventriculomegaly				
UCO-vehicle 4 foetuses	One developed focal unilateral lesions in the temporal lobe One developed focal bilateral cystic lesions in the temporal lobe and the second parasagittal gyrus of the parietal lobe	77.3 ± 7.5	86.3 ± 6.6	1.1 ± 0.8
UCO-Etanercept 2 foetuses	Two developed focal unilateral cystic lesions in the temporal lobe contralateral to the site of intracerebroventricular infusion	101.2 ± 14.9	89.5 ± 2.7	5.6 ± 0.5
Temporal lobe cystic lesions				
UCO-vehicle 3 foetuses	Bilateral lesions Two developed extensive lesions, one developed focal lesions	101.0 ± 12.2	53.1 ± 3.4	17.9 ± 11.7
UCO-Etanercept 2 foetuses	Unilateral focal lesions contralateral to the site of intracerebroventricular infusion	103.7 ± 7.6	66.2 ± 5.2	2.2 ± 1.6
No overt macroscopic features				
UCO-vehicle 2 foetuses	Microscopic diffuse WMI present	126.2 ± 20.3	60.1 ± 5.7	-
UCO-Etanercept 5 foetuses	Microscopic diffuse WMI present	123.7 ± 7.9	67.5 ± 12.9	-

Foetuses were assigned to subgroups based on their primary pattern of macroscopic injury, although overlap between subgroups were observed. No statistical analysis has been performed due to low numbers in each subgroup. Control outcomes are provided for reference. Data are mean ± SEM.

phase can promote severe brain injury.[15] In the present study, TNF blockade was initiated 72 h after HI, after resolution of seizures and other secondary events, at a time when acute WMI is established.[11,15,32] Although neuroinflammation has been widely hypothesized to contribute to the injurious processes of the tertiary phase,[33,34] to the best of our knowledge this is the first direct evidence that modulation of neuroinflammation within the tertiary phase alone can improve severe WMI. This striking finding raises the possibility that cystic WMI in preterm infants might realistically be preventable.[15]

UCO in the present study was associated with a spectrum of WMI after 21 days recovery, similar to our previous report.[11] Severe WMI was predominantly localized to the temporal lobe, and surrounded by diffuse WMI characterized by abnormal myelin protein labelling, oligodendrocyte maturational arrest and microgliosis. Diffuse WMI was also present in the intragyral and periventricular regions of the parietal lobe. We have previously reported that the appearance of severe, macroscopic WMI after HI can be surprisingly delayed, and not seen until 14 to 21 days after UCO.[11] This timing is strikingly parallel to the trajectory of cystic WMI in preterm humans, which typically develops 3–5 weeks after birth on serial cranial ultrasounds,[14,35] albeit more severe cysts tend to appear earlier.[14] Additionally, a subgroup of foetuses in both UCO groups showed marked white matter atrophy with ventricular enlargement that represented the most severe form of macroscopic WMI.[11,15] We speculate that this severe pattern may represent more rapid evolution and subsequent collapse of cystic WMI before 21 days,[15] similar to observations in preterm infants.[7,14] This pattern was less frequent (two versus four foetuses) after Etanercept treatment. Although the area of cystic lesions was greater on average in this subgroup after Etanercept treatment (5.6 ± 0.5 versus 1.1 ± 0.8 mm^2), there was a marked overall improvement in intact white matter area after Etanercept treatment (101.2 ± 14.9 versus 77.3 ± 7.5 mm^2; Table 3). The smaller cystic lesion area in the UCO-vehicle group therefore probably reflects collapse of larger lesions rather than a less severe pattern of injury.

In the present study, multiple lines of evidence support reduced severity of macroscopic WMI after TNF blockade. In the TWM1 region, TNF blockade restored levels of total oligodendrocytes and partially restored MBP-positive myelin protein labelling towards control levels, suggesting greater oligodendrocyte survival and function but persisting impaired oligodendrocyte maturation in the most severely injured region. Further, intact white matter area in the UCO-Etanercept group was intermediate between the control and UCO-vehicle groups, suggesting at least partial restoration of white matter area. We have previously shown in foetal sheep that after intracerebroventricular injection, a small peptide dispersed evenly through both lateral ventricles.[36] Importantly, a large molecule, insulin-like growth factor 1 (7.6 kDa), diffused along the white matter tracts after HI following intracerebroventricular injection in rats.[37,38] In the present study, Etanercept improved outcomes in multiple parietal and temporal lobe white matter regions including sites distal from the lateral ventricles, suggesting that the larger Etanercept protein (150 kDa) overall showed similar distribution. Interestingly, there was greater improvement in TWM1 and greater protection from cystic WMI in the hemisphere ipsilateral to Etanercept infusion than the contralateral hemisphere. This is consistent with a direct beneficial effect of Etanercept treatment but does suggest that the concentration of Etanercept reaching the contralateral temporal lobe was insufficient to completely attenuate the severe injury in this region. Future studies should examine whether this can be overcome by a larger dose or whether bilateral infusions are essential.

TNF blockade was started 72 h after UCO, after the end of the secondary phase of injury, at a time when current understanding suggests that most of all HI cell death is established.[32] Consistent with this, we have previously reported little change in white matter cell death from 3 to 7 days after HI.[11] Thus, the improvement in WMI in the present study after delayed treatment suggests that tertiary cell death was mediated by delayed local TNF production and subsequent activation of downstream inflammatory and cell death pathways, rather than propagation of injurious pathways initiated

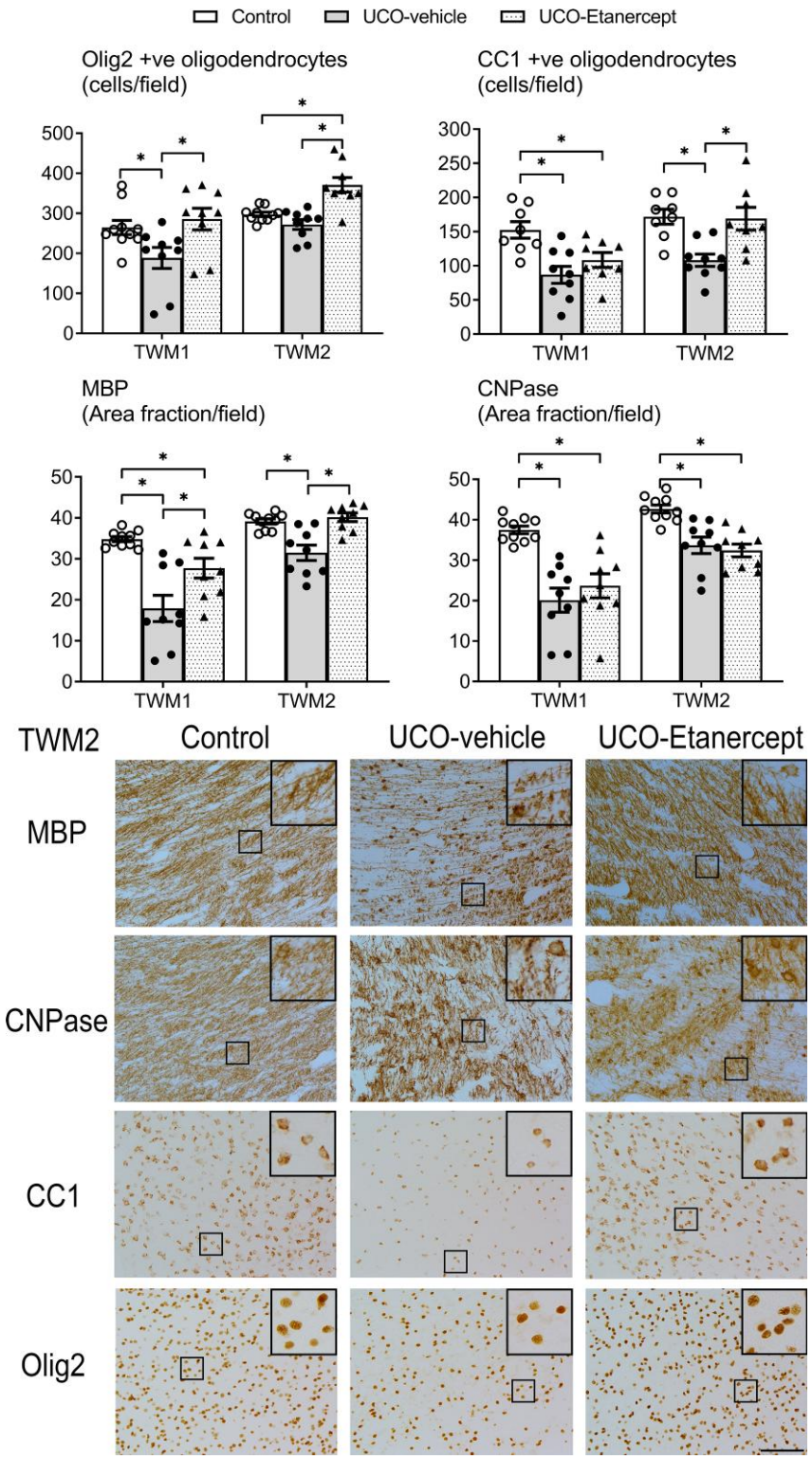

Figure 2 Temporal lobe WMI. *Top panels* show the numbers of total (Olig-2) and mature (CC1) oligodendrocytes and the area fractions of two myelin proteins (MBP and CNPase) in the TWM regions (TWM1 and TWM2). Asterisk denotes significant difference of $P < 0.05$ between the two groups indicated. Data are means ± SEM. *Bottom panels* show the representative photomicrographs of MBP-positive and CNPase-positive labelling and total (Olig2) and mature (CC1) oligodendrocytes in the TWM2 region. Note the sparse labelling of myelin proteins with abnormal morphology in the UCO-vehicle group. Improved myelin protein morphology is observed in the UCO-Etanercept group, more closely resembling that observed in the control group. All images were taken at ×20 magnification, *insets* are ×3 enlargements. Scale bar = 100 µm.

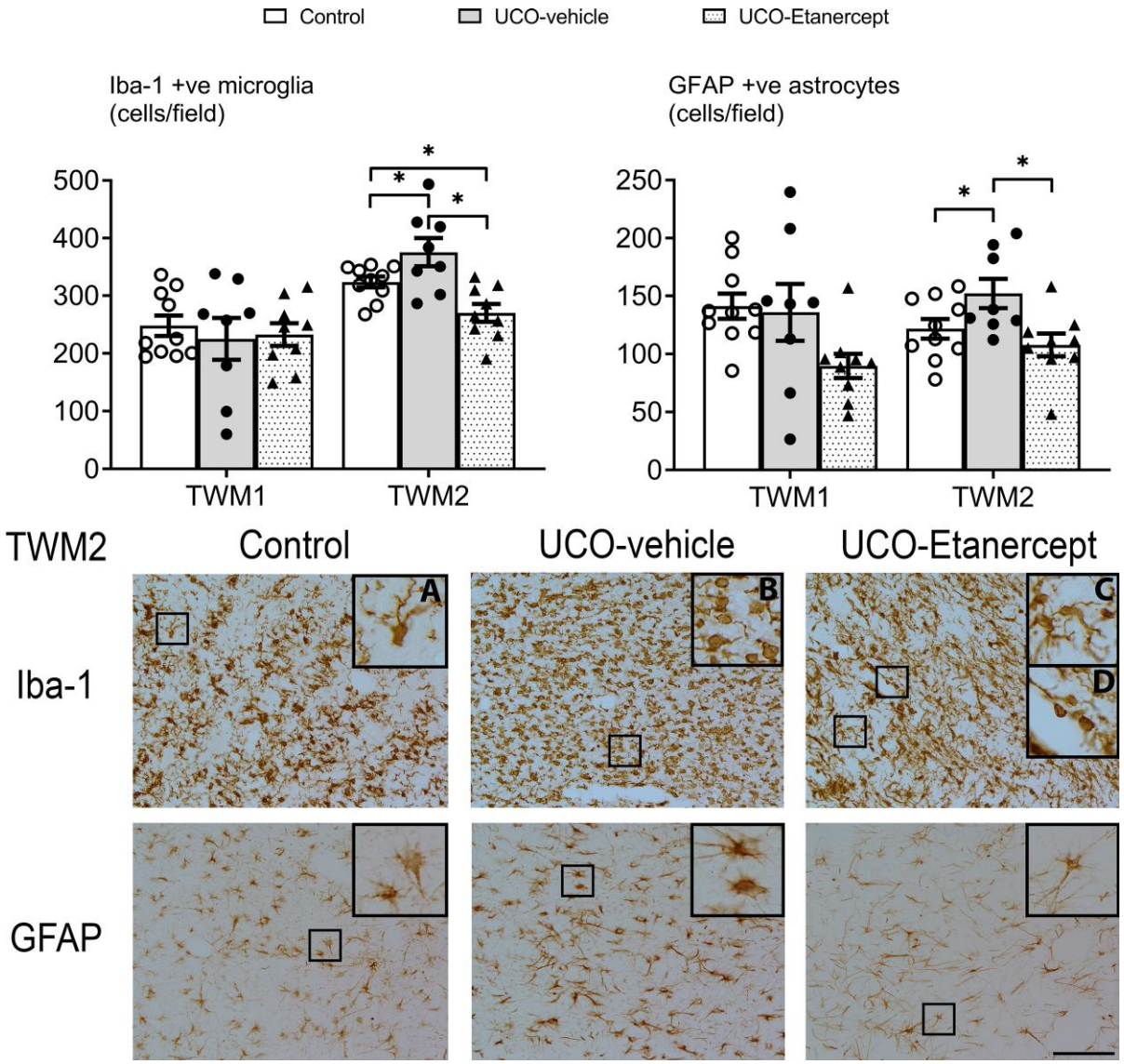

Figure 3 Temporal lobe white matter neuroinflammation. *Top panels* show the numbers of microglia (Iba-1) and astrocytes (GFAP) in the TWM regions (TWM1 and TWM2). Asterisk denotes significant difference of $P < 0.05$ between the two groups indicated. Data are means ± SEM. *Bottom panels* show the representative photomicrographs of microglia (Iba-1) and astrocytes (GFAP) in the TWM2 region. Note the profound decrease in microglia density, as well as a more subtle decrease in astrocyte density in the UCO-Etanercept group. All images were taken at ×20 magnification, *insets* are ×3 enlargements. (**A**) Example of ramified microglia in the control group. (**B**) Example of amoeboid microglia in the UCO-vehicle group. (**C**) Examples of ramified microglia and (**D**) amoeboid microglia in the UCO-Etanercept group. Scale bar = 100 µm.

during acute HI. Excessive TNF can initiate programmed necrosis in neonatal rats,[16,17] leading to very delayed cell death.[39,40] We have previously reported in the same model that severe WMI was spatially associated with local aggregates of microglia in the same regions before the onset of tertiary cell death.[11] These structures of densely packed amoeboid microglia are important in axonal guiding and pruning and form around axonal crossroads at 19–24 gestational weeks in humans, but have also been associated with areas of greater WMI in humans.[13,41] Etanercept may have mitigated temporal lobe WMI by attenuating excessive neuroinflammation and TNF production originating from these microglial aggregates. The beneficial effects of Etanercept given at Days 3, 8 and 13 after UCO is broadly consistent with the concept that excessive TNF production contributed to tertiary cell death between 3 and 14 days after UCO. Further studies will be required to precisely understand the trajectory of TNF production after UCO. Understanding the evolution of microglial phenotypes over the tertiary phase in regions of cystic and diffuse injury is likewise a crucial topic for future studies but, unfortunately, we have been unable to assess microglial phenotypes in the present tissue due to technical constraints.

The present study further emphasizes the marked variability of WMI after severe HI in the preterm brain. It is interesting that the pattern of injury in the present paradigm of 25 min of UCO is much more consistent at 3–7 days than after 14–21 days recovery.[11] In the present study, the variability of WMI did not appear to be related to hypotension during HI, despite hypotension being known to be a key determinant of neuronal injury following HI.[42–44] Speculatively, variability in the location, size and activity of microglial aggregates at the time of HI (and therefore severe arterial hypotension) may contribute to the variability of eventual WMI.

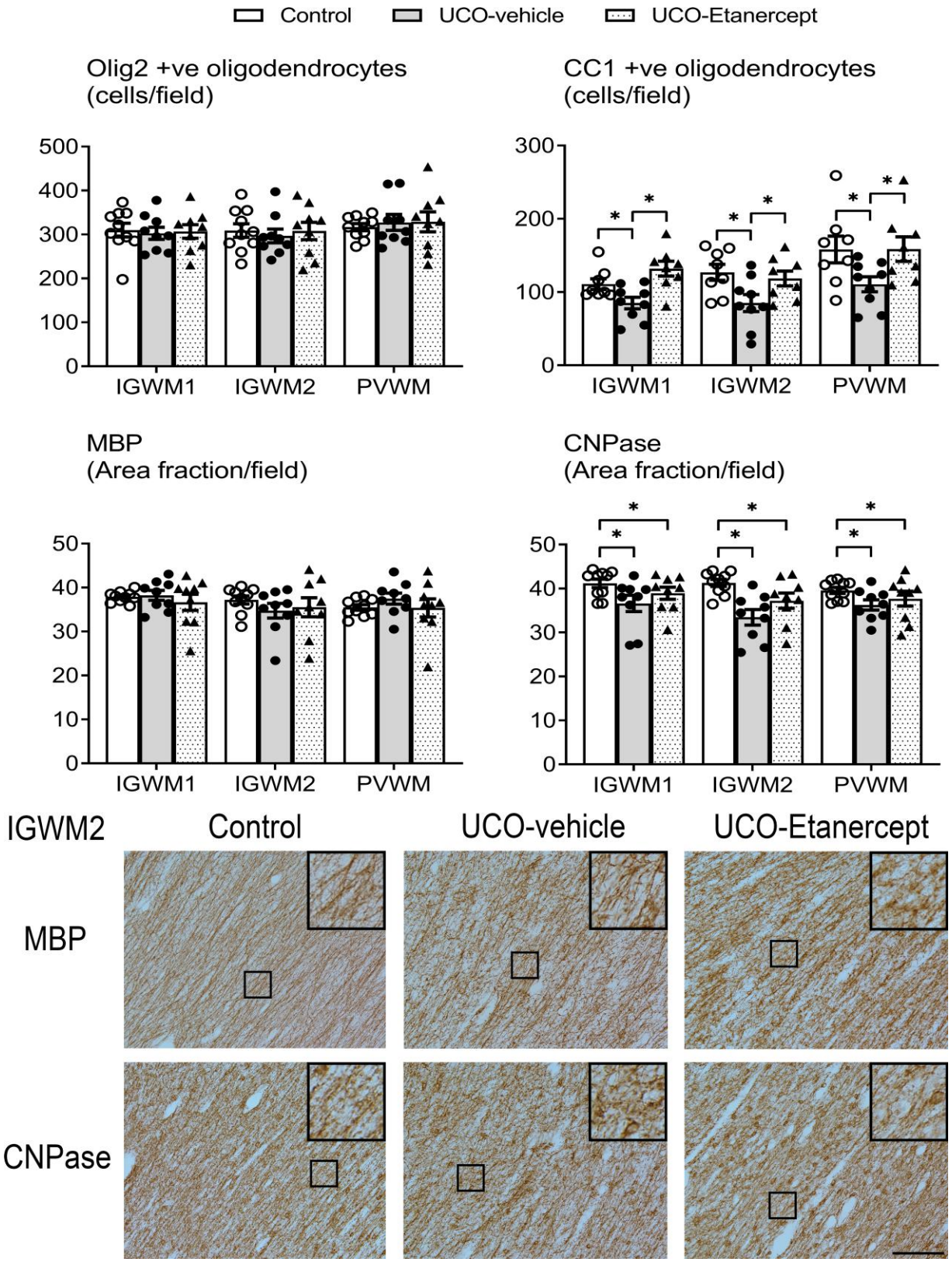

Figure 4 Parietal lobe WMI. *Top panels* show the numbers of total (Olig-2) and mature (CC1) oligodendrocytes and the area fractions of two myelin proteins (MBP and CNPase) in the parietal white matter regions (IGWM1/2 and PVWM). Asterisk denotes significant difference of $P < 0.05$ between the two groups indicated. Data are means ± SEM. *Bottom panels* show the representative photomicrographs of MBP-positive and CNPase-positive labelling in the IGWM2 region. Note the near-normal intensity and morphology of myelin protein labelling in both the UCO-vehicle and UCO-Etanercept groups, closely resembling that observed in the control group. All images were taken at ×20 magnification, *insets* are ×3 enlargements. Scale bar = 100 µm.

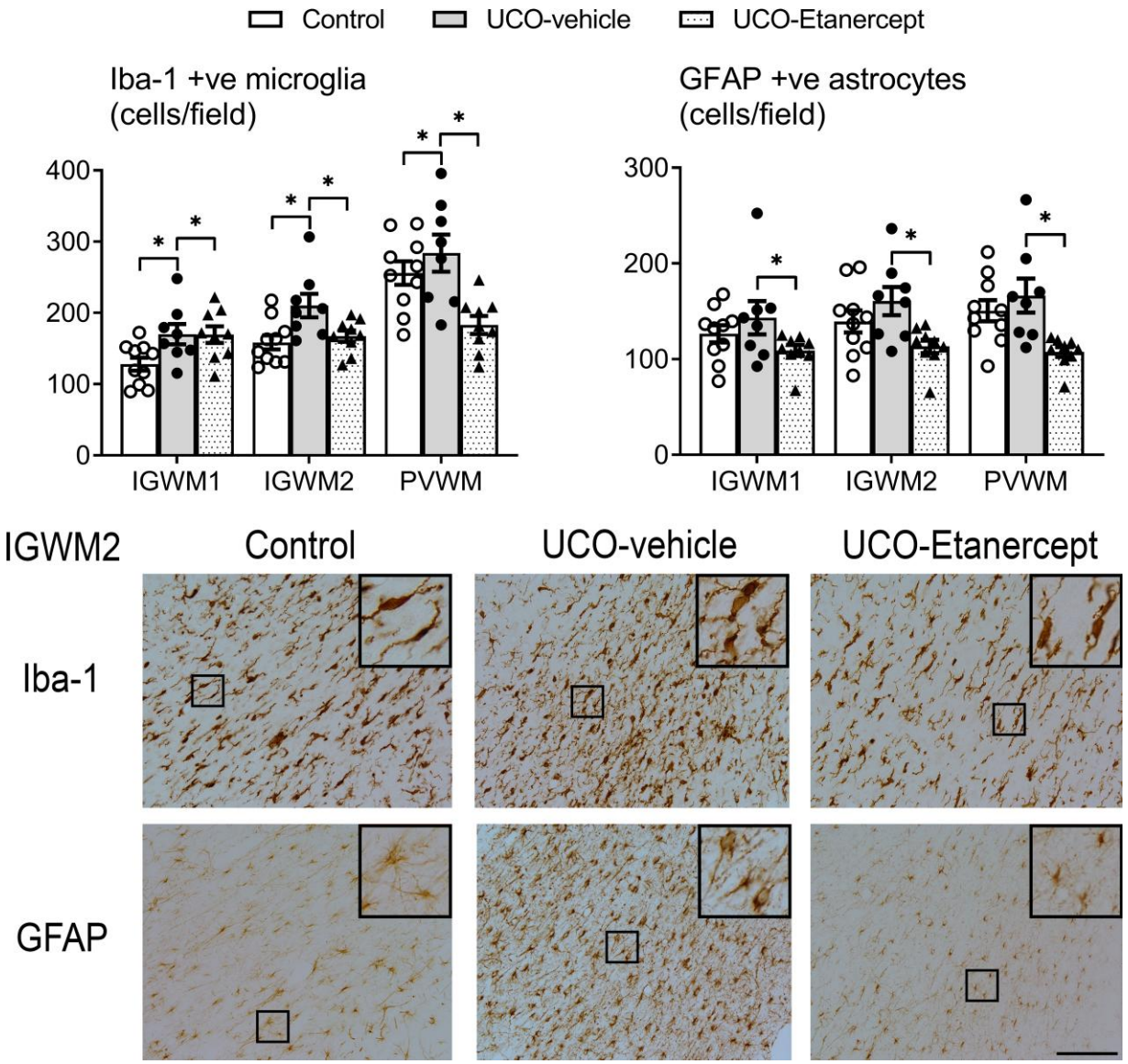

Figure 5 Parietal lobe white matter neuroinflammation. *Top panels* show the numbers of microglia (Iba-1) and astrocytes (GFAP) in the parietal white matter regions (IGWM1/2 and PVWM). Asterisk denotes significant difference of $P < 0.05$ between the two groups indicated. Data are means ± SEM. *Bottom panels* show the representative photomicrographs of Iba-1-positive microglia and GFAP-positive astrocytes in the IGWM2 region. Note the profound reduction in both microglia and astrocyte density in the UCO-Etanercept group back to control levels. Micrographs also display a similar proportion of ramified to amoeboid microglia morphology between UCO-Etanercept and the control group. All images were taken at ×20 magnification, *insets* are ×3 enlargements. Scale bar = 100 µm.

Furthermore, given the key role of inflammation in the pathogenesis of cystic WMI, it is plausible that genetic, antenatal, intrapartum and postnatal events that modulate inflammation may also affect the risk of cystic WMI after HI. Such complex interactions may contribute to the variability in WMI observed in the human preterm infant.

Improved recovery of diffuse white matter injury

Contemporary post-mortem cohort studies in extremely preterm infants have consistently shown the presence of diffuse non-cystic WMI with astrogliosis, maturational arrest of oligodendrocytes and impaired myelination.[5,6,45,46] In the absence of necrotic lesions, this diffuse WMI appears to be a key driver of mild-moderate neurodevelopmental impairment.[9] In the present study, relatively diffuse WMI was observed in the UCO-vehicle group in the TWM2 region including oligodendrocyte maturational arrest, with increased numbers of total oligodendrocytes (Olig2-positive) but reduced numbers of mature oligodendrocytes (CC1-positive), reduced and morphologically abnormal MBP-positive and CNPase-positive myelin protein labelling, and increased numbers of morphologically activated microglia, consistent with previous studies.[45,47–50] TNF blockade markedly mitigated the severity of this diffuse WMI. Increased numbers of total oligodendrocytes were still observed after TNF blockade, suggesting it did not alter restorative proliferation after HI[47]; however, the improvement in the numbers of mature oligodendrocytes to control levels denotes improved oligodendrocyte maturation. Further, MBP-positive labelling

in the TWM2 region was restored to control levels, confirming improved oligodendrocyte function. Interestingly, CNPase-positive labelling, which represents ~4% of the myelin sheath, was not similarly restored. A similar differential improvement in MBP-positive over CNPase-positive labelling is observed with hypothermic neuroprotection after ischaemia in near-term foetal sheep.[51] The mechanism and potential implications of this differential protection is unknown.

Milder diffuse WMI injury was also present in the parietal lobe in the UCO-vehicle group, with reduced numbers of mature oligodendrocytes and increased microglia. Although CNPase-positive myelin protein labelling was impaired, MBP-positive labelling was both quantitatively and morphologically normal. This is consistent with our recent longitudinal analysis which illustrated that myelin protein labelling remains impaired in the same parietal lobe regions for 14 days after UCO, but shows surprising recovery by 21 days.[11]

Notably, TNF blockade in the present study also restored the levels of mature oligodendrocytes in the parietal lobe, supporting the concept that persisting neuroinflammation after perinatal HI contributes to oligodendrocyte maturational arrest and impaired myelination.[34] To the best of our knowledge, this is the first direct demonstration that modulating neuroinflammation during the tertiary phase alone can improve oligodendrocyte maturation associated with diffuse WMI. Further, Etanercept attenuated the increased numbers of both microglia and astrocytes in the regions of diffuse WMI and was even associated with a striking reduction in microglia below control levels in the TWM2 region. It is not possible to determine from the present study whether the beneficial effects on diffuse WMI were mediated by the direct effects of TNF blockade or indirectly via reduced numbers or activation of local glia cells; it is plausible that both mechanisms may be important. It is also possible that less severe injury within the TWM1 region after TNF blockade may also have had beneficial feedforward effects on the recovery and maturation of the TWM2 region and the more distant parietal lobe white matter regions, for example, through reduced axonal degeneration and improved inter-region connectivity. The implications of the marked reduction in microglial levels below control levels in the TWM2 region are unknown, and both microglia and TNF have important roles in neurodevelopment.[13,41,52] In future studies it will be important to examine whether TNF blockade may have unintended adverse neurodevelopmental effects, especially after milder cases of HI when the benefit to risk profile may be substantially different.

Significance and perspectives

The present study supports the concept that a key mechanism of cystic WMI is slowly evolving programmed necrosis stimulated by delayed, exuberant local neuroinflammation and TNF production, rather than non-modifiable injury sustained during the initial period of HI. The mitigation of both cystic and diffuse WMI following TNF blockade in the present study suggests the tantalizing possibility that substantial white matter protection may be possible in preterm humans with even very delayed treatment strategies.[15] Of interest, a Trojan-horse Etanercept molecule that can pass the blood–brain barrier is in development.[21] Regardless, further pragmatic studies are needed to optimize the dose and timing of TNF blockade, as well as investigate therapeutic options that can be delivered systemically.

Acknowledgements

The graphic abstract figure was created with Biorender.com.

Funding

This study was funded by grants from the Health Research Council of New Zealand (grant numbers 17/601, 20/437, 22/559). The funding sources had no role in the conception, writing or decision to submit this review for publication.

Competing interests

The authors report no competing interests.

Supplementary material

Supplementary material is available at *Brain* online.

References

1. Galea C, McIntyre S, Smithers-Sheedy H, *et al*. Cerebral palsy trends in Australia (1995–2009): A population-based observational study. *Dev Med Child Neurol*. 2019;61:186-193.
2. Ghotra S, Vincer M, Allen VM, Khan N. A population-based study of cystic white matter injury on ultrasound in very preterm infants born over two decades in Nova Scotia, Canada. *J Perinatol*. 2019;39:269-277.
3. Banker BQ, Larroche JC. Periventricular leukomalacia of infancy. A form of neonatal anoxic encephalopathy. *Arch Neurol*. 1962;7:386-410.
4. Hamrick SE, Miller SP, Leonard C, *et al*. Trends in severe brain injury and neurodevelopmental outcome in premature newborn infants: The role of cystic periventricular leukomalacia. *J Pediatr*. 2004;145:593-599.
5. Gano D, Andersen SK, Partridge JC, *et al*. Diminished white matter injury over time in a cohort of premature newborns. *J Pediatr*. 2015;166:39-43.
6. van Haastert IC, Groenendaal F, Uiterwaal CS, *et al*. Decreasing incidence and severity of cerebral palsy in prematurely born children. *J Pediatr*. 2011;159:86-91.e1.
7. Sarkar S, Shankaran S, Barks J, *et al*. Outcome of preterm infants with transient cystic periventricular leukomalacia on serial cranial imaging up to term equivalent age. *J Pediatr*. 2018;195:59-65 e3.
8. Galinsky R, Lear CA, Dean JM, *et al*. Complex interactions between hypoxia-ischemia and inflammation in preterm brain injury. *Dev Med Child Neurol*. 2018;60:126-133.
9. Back SA. White matter injury in the preterm infant: Pathology and mechanisms. *Acta Neuropathol*. 2017;134:331-349.
10. Manuck TA, Rice MM, Bailit JL, *et al*. Preterm neonatal morbidity and mortality by gestational age: A contemporary cohort. *Am J Obstet Gynecol*. 2016;215:103.e1-103.e14.
11. Lear BA, Lear CA, Davidson JO, *et al*. Tertiary cystic white matter injury as a potential phenomenon after hypoxia-ischaemia in preterm fetal sheep. *Brain Commun*. 2021;3:fcab024.
12. Schneider J, Miller SP. Preterm brain injury: White matter injury. *Handb Clin Neurol*. 2019;162:155-172.
13. Verney C, Pogledic I, Biran V, Adle-Biassette H, Fallet-Bianco C, Gressens P. Microglial reaction in axonal crossroads is a hallmark of noncystic periventricular white matter injury in very preterm infants. *J Neuropathol Exp Neurol*. 2012;71:251-264.
14. Pierrat V, Duquennoy C, van Haastert IC, Ernst M, Guilley N, de Vries LS. Ultrasound diagnosis and neurodevelopmental

outcome of localised and extensive cystic periventricular leucomalacia. *Arch Dis Child Fetal Neonatal Ed*. 2001;84:F151-F156.
15. Lear BA, Lear CA, Dhillon SK, Davidson JO, Bennet L, Gunn AJ. Is late prevention of cerebral palsy in extremely preterm infants plausible? *Dev Neurosci*. 2022;44:177-185.
16. Thornton C, Leaw B, Mallard C, Nair S, Jinnai M, Hagberg H. Cell death in the developing brain after hypoxia-ischemia. *Front Cell Neurosci*. 2017;11:248.
17. Northington FJ, Chavez-Valdez R, Graham EM, Razdan S, Gauda EB, Martin LJ. Necrostatin decreases oxidative damage, inflammation, and injury after neonatal HI. *J Cereb Blood Flow Metab*. 2011;31:178-189.
18. McIntosh GH, Baghurst KI, Potter BJ, Hetzel BS. Foetal brain development in the sheep. *Neuropathol Appl Neurobiol*. 1979;5:103-114.
19. Back SA, Riddle A, Dean J, Hohimer AR. The instrumented fetal sheep as a model of cerebral white matter injury in the premature infant. *Neurotherapeutics*. 2012;9:359-370.
20. Tracey D, Klareskog L, Sasso EH, Salfeld JG, Tak PP. Tumor necrosis factor antagonist mechanisms of action: a comprehensive review. *Pharmacol Ther*. 2008;117:244-279.
21. Sumbria RK, Boado RJ, Pardridge WM. Brain protection from stroke with intravenous TNFα decoy receptor-trojan horse fusion protein. *J Cereb Blood Flow Metab*. 2012;32:1933-1938.
22. du Sert N P, Hurst V, Ahluwalia A, *et al*. The ARRIVE guidelines 2.0: Updated guidelines for reporting animal research. *J Physiol*. 2020;598:3793-3801.
23. Lear CA, Kasai M, Booth LC, *et al*. Peripheral chemoreflex control of fetal heart rate decelerations overwhelms the baroreflex during brief umbilical cord occlusions in fetal sheep. *J Physiol*. 2020; 598:4523-4536.
24. Lear CA, Koome MM, Davidson JO, *et al*. The effects of dexamethasone on post-asphyxial cerebral oxygenation in the preterm fetal sheep. *J Physiol*. 2014;592:5493-5505.
25. Bennet L, Roelfsema V, Pathipati P, Quaedackers J, Gunn AJ. Relationship between evolving epileptiform activity and delayed loss of mitochondrial activity after asphyxia measured by near-infrared spectroscopy in preterm fetal sheep. *J Physiol*. 2006;572:141-154.
26. Nestorov I, Zitnik R, DeVries T, Nakanishi AM, Wang A, Banfield C. Pharmacokinetics of subcutaneously administered etanercept in subjects with psoriasis. *Br J Clin Pharmacol*. 2006;62:435-445.
27. Aden U, Favrais G, Plaisant F, *et al*. Systemic inflammation sensitizes the neonatal brain to excitotoxicity through a pro-/anti-inflammatory imbalance: Key role of TNFalpha pathway and protection by etanercept. *Brain Behav Immun*. 2010;24:747-758.
28. Ralph SJ, Weissenberger A, Bonev V, *et al*. Phase I/II parallel double-blind randomized controlled clinical trial of perispinal etanercept for chronic stroke: Improved mobility and pain alleviation. *Expert Opin Investig Drugs*. 2020;29:311-326.
29. Gluckman PD, Parsons Y. Stereotaxic method and atlas for the ovine fetal forebrain. *J Dev Physiol*. 1983;5:101-128.
30. Lear CA, Davidson JO, Mackay GR, *et al*. Antenatal dexamethasone before asphyxia promotes cystic neural injury in preterm fetal sheep by inducing hyperglycemia. *J Cereb Blood Flow Metab*. 2018;38:706-718.
31. Dhillon SK, Wassink G, Lear CA, Davidson JO, Gunn AJ, Bennet L. Adverse neural effects of delayed intermittent treatment with rEPO after asphyxia in preterm fetal sheep. *J Physiol*. 2021;599: 3593-3609.
32. Dhillon SK, Lear CA, Galinsky R, *et al*. The fetus at the tipping point: modifying the outcome of fetal asphyxia. *J Physiol*. 2018; 596:5571-5592.
33. Fleiss B, Gressens P. Tertiary mechanisms of brain damage: A new hope for treatment of cerebral palsy? *Lancet Neurol*. 2012; 11:556-566.
34. Prasad JD, Gunn KC, Davidson JO, *et al*. Anti-inflammatory therapies for treatment of inflammation-related preterm brain injury. *Int J Mol Sci* 2021; 22: 4008.
35. Hayakawa F, Okumura A, Kato T, Kuno K, Watanabe K. Determination of timing of brain injury in preterm infants with periventricular leukomalacia with serial neonatal electroencephalography. *Pediatrics*. 1999;104:1077-1081.
36. Davidson JO, Green CR, Nicholson LFB, *et al*. Connexin hemichannel blockade improves outcomes in a model of fetal ischemia. *Ann Neurol*. 2012;71:121-132.
37. Guan J, Beilharz EJ, Skinner SJ, Williams CE, Gluckman PD. Intracerebral transportation and cellular localisation of insulin-like growth factor-1 following central administration to rats with hypoxic-ischemic brain injury. *Brain Res*. 2000; 853:163-173.
38. Guan J, Skinner SJ, Beilharz EJ, *et al*. The movement of IGF-I into the brain parenchyma after hypoxic-ischaemic injury. *Neuroreport*. 1996;7:632-636.
39. Northington FJ, Chavez-Valdez R, Graham EM, Razdan S, Gauda EB, Martin LJ. Necrostatin decreases oxidative damage, inflammation, and injury after neonatal HI. *J Cereb Blood Flow Metab*. 2011;31:178-189. Epub Jun 23.
40. Stone BS, Zhang J, Mack DW, Mori S, Martin LJ, Northington FJ. Delayed neural network degeneration after neonatal hypoxia-ischemia. *Ann Neurol*. 2008;64:535-546.
41. Pierre WC, Smith PL, Londono I, Chemtob S, Mallard C, Lodygensky GA. Neonatal microglia: The cornerstone of brain fate. *Brain Behav Immun*. 2017;59:333-345.
42. Ikeda T, Murata Y, Quilligan EJ, *et al*. Physiologic and histologic changes in near-term fetal lambs exposed to asphyxia by partial umbilical cord occlusion. *Am J Obstet Gynecol*. 1998;178: 24-32.
43. Gunn AJ, Parer JT, Mallard EC, Williams CE, Gluckman PD. Cerebral histologic and electrocorticographic changes after asphyxia in fetal sheep. *Pediatr Res*. 1992;31:486-491.
44. Lear CA, Kasai M, Drury PP, *et al*. Plasma vasopressin levels are closely associated with fetal hypotension and neuronal injury after hypoxia-ischemia in near-term fetal sheep. *Pediatr Res*. 2020;88:857-864.
45. Buser JR, Maire J, Riddle A, *et al*. Arrested preoligodendrocyte maturation contributes to myelination failure in premature infants. *Ann Neurol*. 2012;71:93-109.
46. Reid SM, Meehan E, McIntyre S, Goldsmith S, Badawi N, Reddihough DS. Temporal trends in cerebral palsy by impairment severity and birth gestation. *Dev Med Child Neurol*. 2016; 58:25-35.
47. Segovia KN, McClure M, Moravec M, *et al*. Arrested oligodendrocyte lineage maturation in chronic perinatal white matter injury. *Ann Neurol*. 2008;63:520-530.
48. Riddle A, Dean J, Buser JR, *et al*. Histopathological correlates of magnetic resonance imaging-defined chronic perinatal white matter injury. *Ann Neurol*. 2011;70:493-507.
49. Drury PP, Davidson JO, Bennet L, *et al*. Partial neural protection with prophylactic low-dose melatonin after asphyxia in preterm fetal sheep. *J Cereb Blood Flow Metab*. 2014;34: 126-135.
50. Galinsky R, Draghi V, Wassink G, *et al*. Magnesium sulfate reduces EEG activity but is not neuroprotective after asphyxia in preterm fetal sheep. *J Cereb Blood Flow Metab*. 2017;37: 1362-1373.
51. Draghi V, Wassink G, Zhou KQ, Bennet L, Gunn AJ, Davidson JO. Differential effects of slow rewarming after cerebral hypothermia on white matter recovery after global cerebral ischemia in near-term fetal sheep. *Sci Rep*. 2019;9:10142.
52. Deverman BE, Patterson PH. Cytokines and CNS development. *Neuron*. 2009;64:61-78.